Electronic Supplementary Material (ESI) for Journal of Materials Chemistry A.
This journal is © The Royal Society of Chemistry 2023

Supporting information

Enhancing Li ions conduction through polyethylene glycol brushes towards long-life solid-state lithium metal batteries

*Yuxuan Li, Jing Yang, Xingzhao Zhang, Ximing Cui, and Qinmin Pan**

(School of Chemistry and Chemical Engineering, Harbin Institute of Technology, Harbin 150001, P. R. China)

Qinmin Pan

State Key Laboratory of Robotics and Systems

School of Chemistry and Chemical Engineering

Harbin Institute of Technology, Harbin 150001, *P. R.* China

E-mail: panqm@hit.edu.cn

Table of Contents

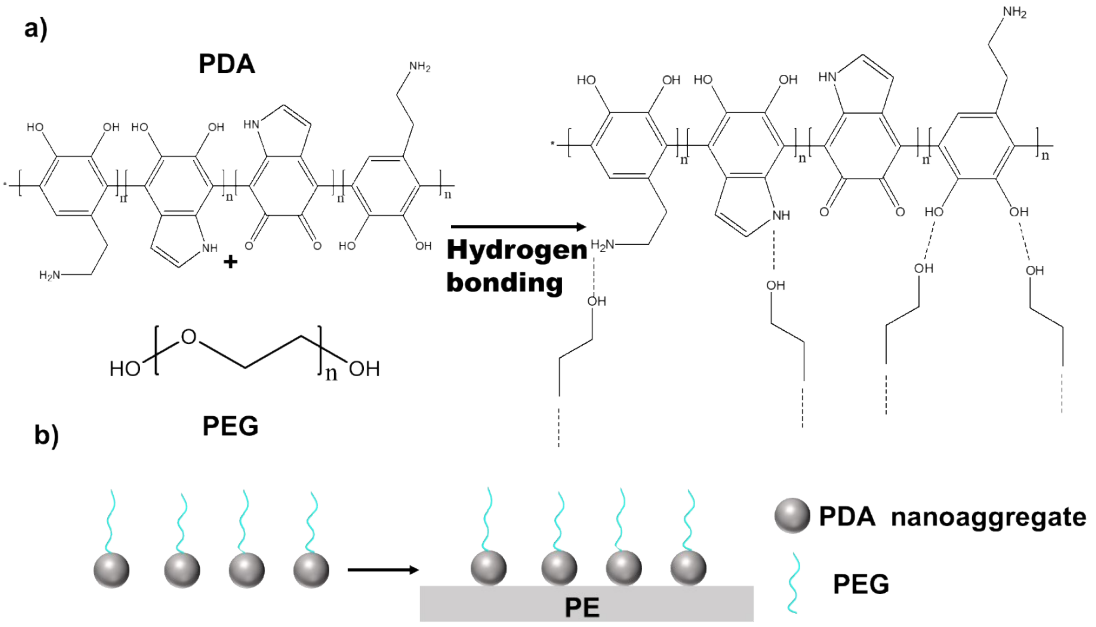

Fig. S1 The self-assembly process of the PEG brushes on the PE-PEG separator. a) The interaction between PDA and PEG through hydrogen bonding. b) Illustration of possible structure for the PE-PEG separator.

Fig. S2 depicts the photographs of the liquid precursor and SN-based electrolyte (SNE). It is found that the liquid precursor is cured after the thermal polymerization.

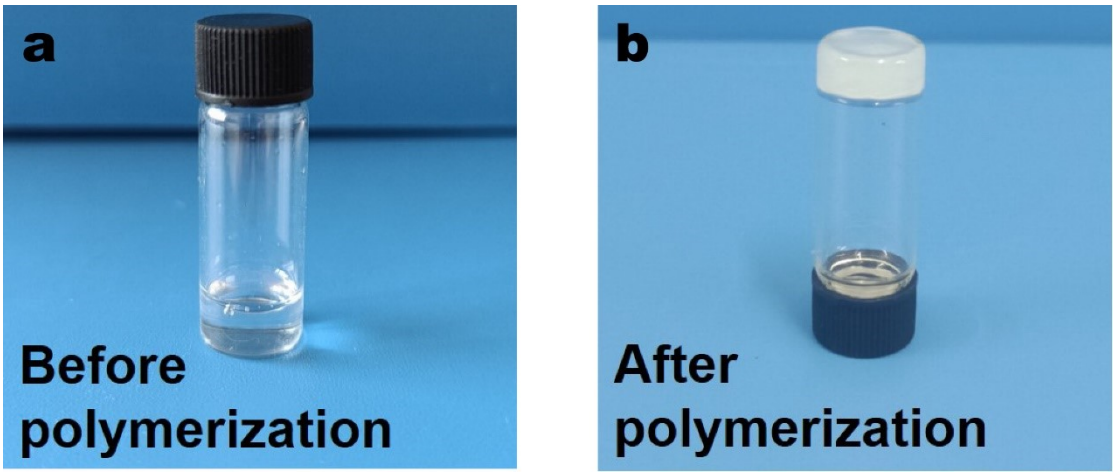

Fig. S2 Photographs of the liquid precursor (SN/ETPTA/LiTFSI/FEC/AIBN). a) before and b) after polymerization.

Thermogravimetry (TG) and differential scanning calorimetry (DSC) were conducted to investigate thermal properties of SNE (Fig. S3). As shown in Fig. S3a, the SNE is thermally stable over 117 ^{o}C. The DSC plot shows an endothermic peaks at −41.8 ^{o}C, which is assigned to the transition temperature from crystal to plastic crystal of SNE (Fig. S3b).

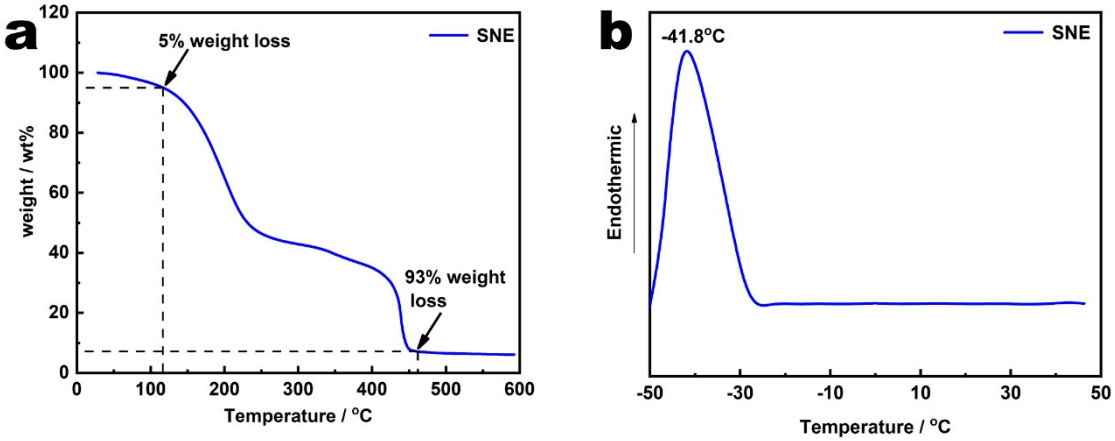

Fig. S3 Thermogravimetric analysis of SNE. a) Thermogravimetric curve and b) DSC curve of SNE.

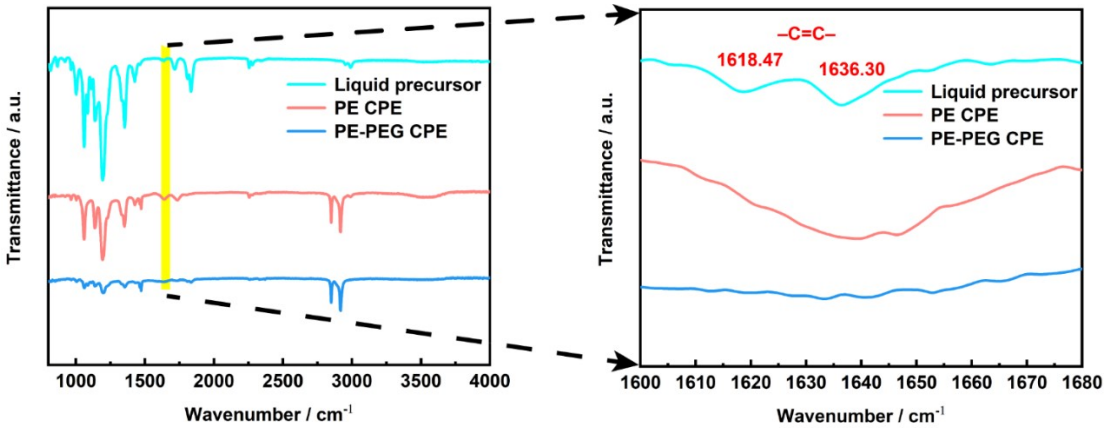

Fig. S4 FTIR spectra of the liquid precursor (SN/ETPTA/LiTFSI/FEC/AIBN), PE CPE and PE-PEG CPE.

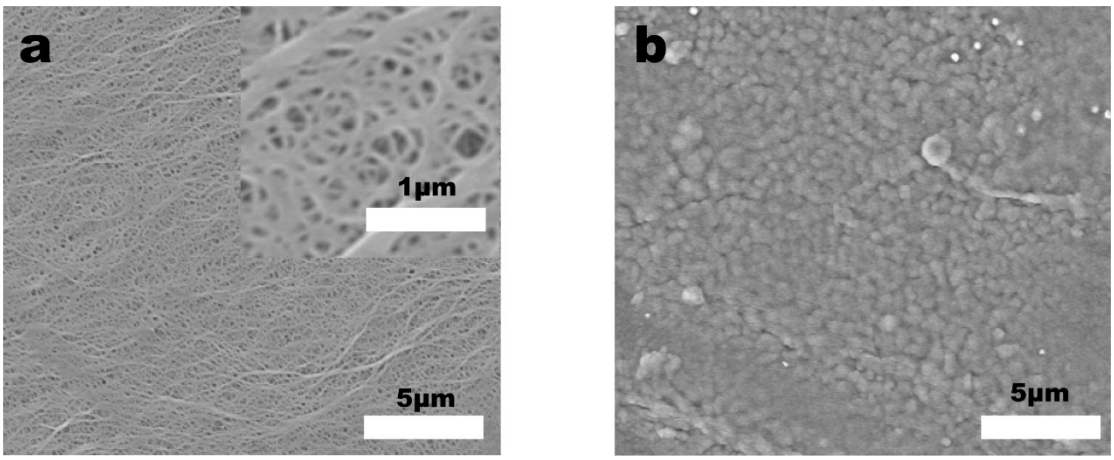

Fig. S5 SEM images and photographs (inset) of the a) PE separator and b) PE CPE.

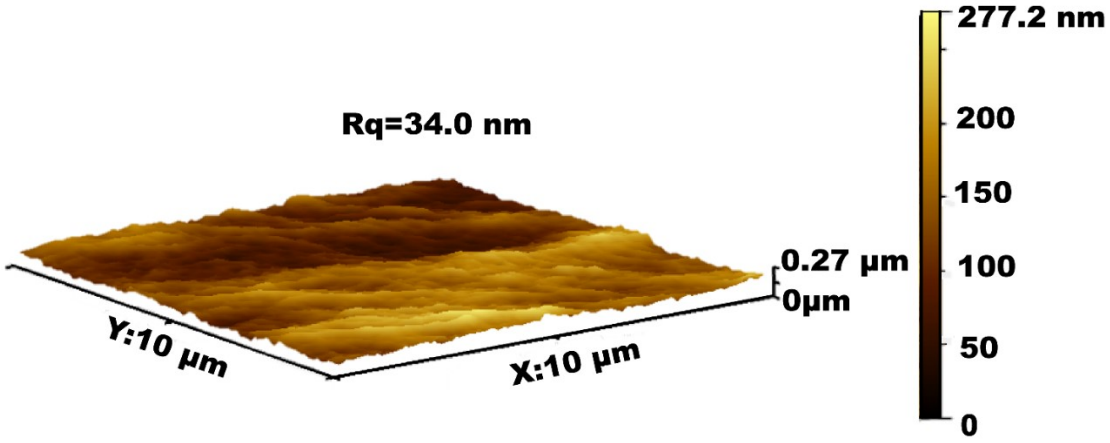

Fig. S6 AFM image and the corresponding roughness of PE separator.

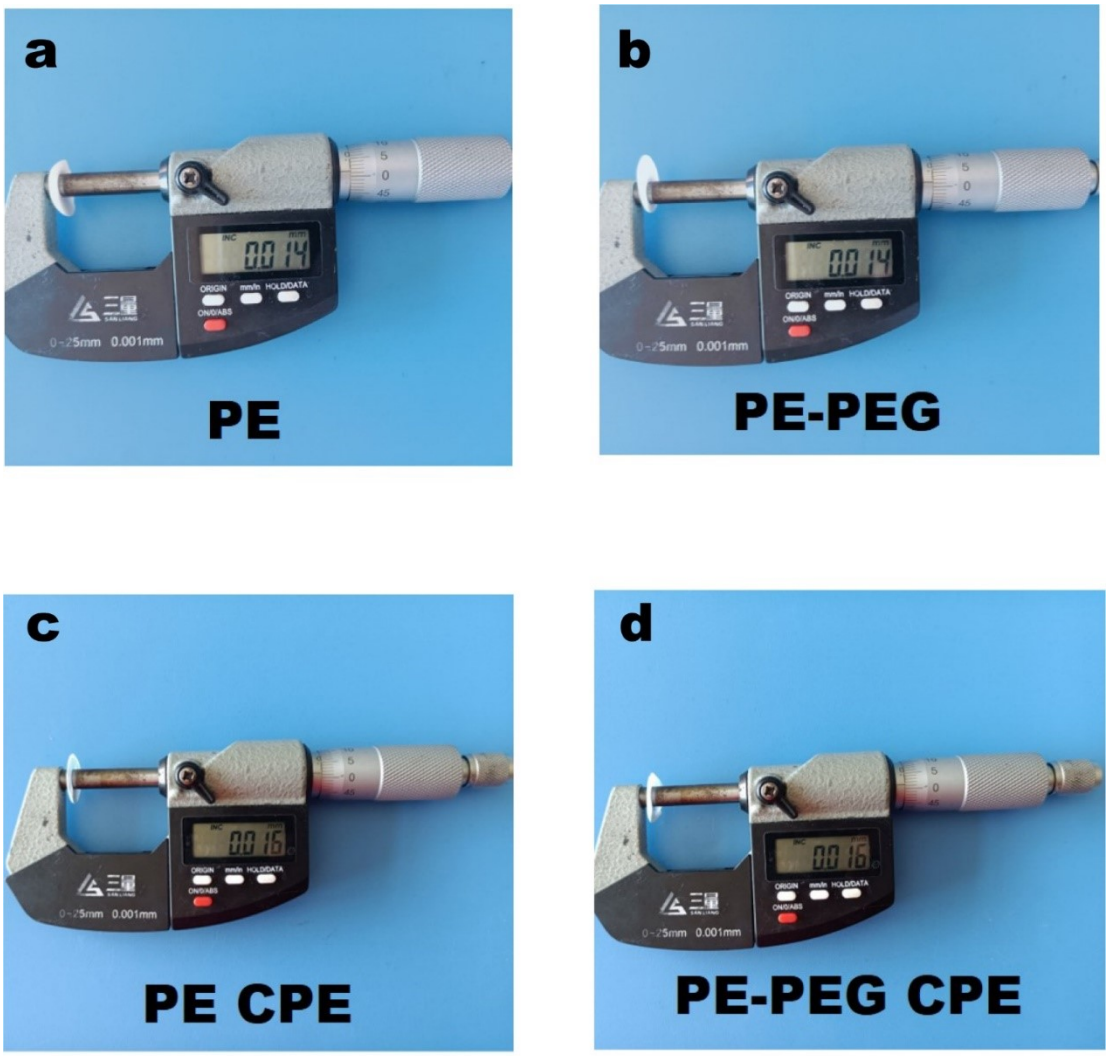

Fig. S7 The thickness of the a) PE separator and b) PE-PEG separator, c) PE CPE and d) PE-PEG CPE.

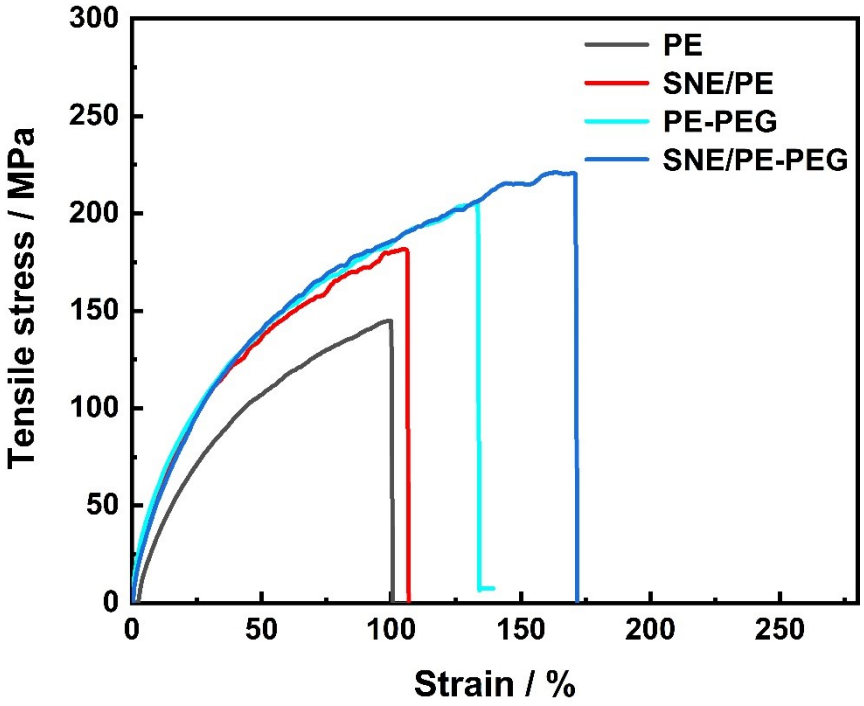

Fig. S8 Tensile stress-strain curves of the PE, PE-PEG separators, PE CPE and PE-PEG CPE.

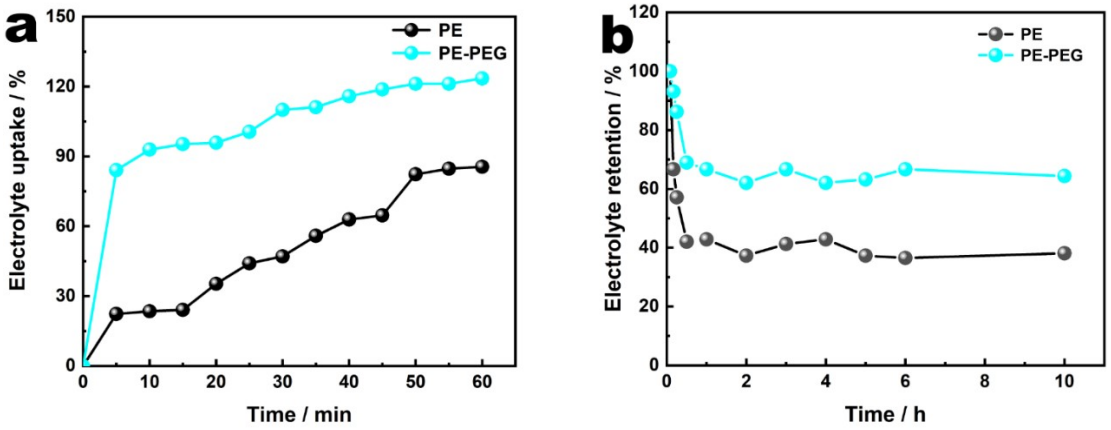

Fig. S9 (a) The electrolyte uptake ability and (b) electrolyte retention capability of different separators.

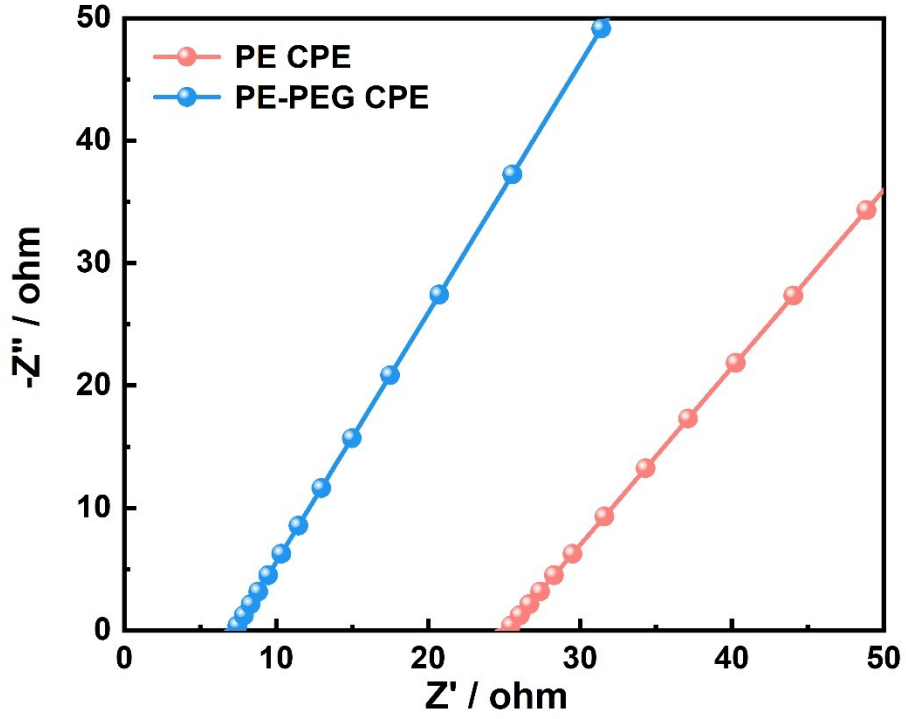

Fig. S10 Nyquist plots of PE CPE and PE-PEG CPE at 30°C.

The conductivities of PE-PEG CPE, PE-PEG4000 CPE and PE-PEG600000 CPE reached respectively 1.07×10^{-4}, 0.84×10^{-4} and 0.81×10^{-4} S cm^{-1} at 30°C and are much higher than the value the PE CPE (0.32×10^{-4} S cm^{-1}) . In this study, the molecular (20000) of PEG is selected for further study due to its higher conductivity.

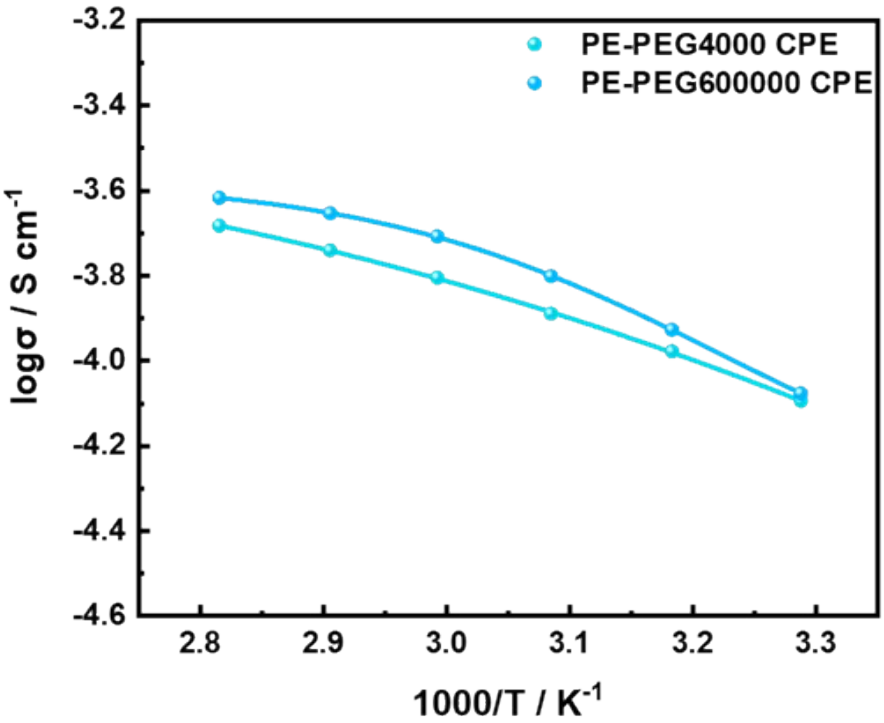

Fig. S11 Ionic conductivity of PE-PEG4000 CPE, PE-PEG600000 CPE in the temperature ranging from 30 to 80 °C.

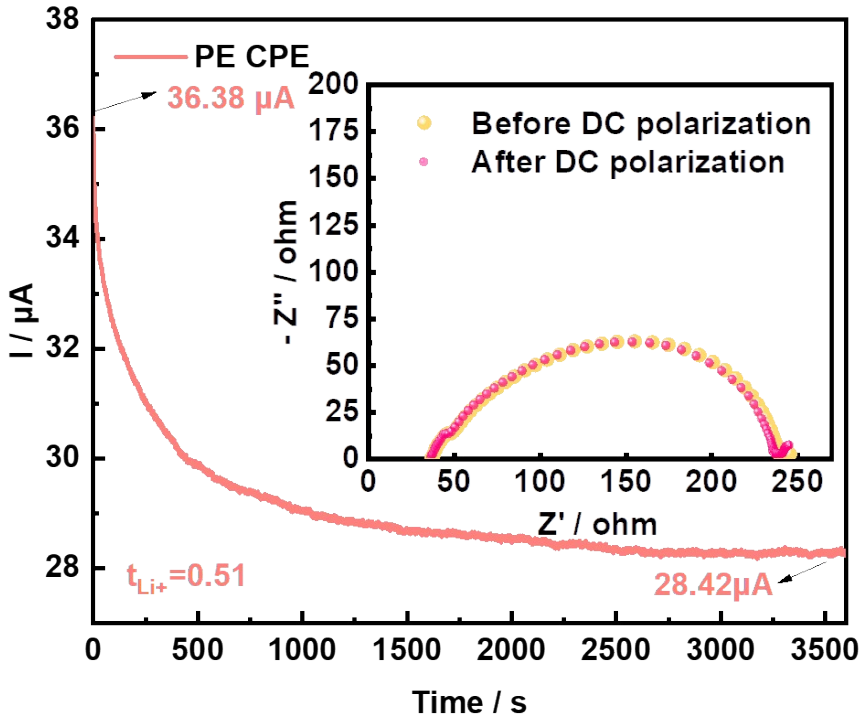

Fig. S12 Chronoamperometric plot of the Li symmetrical cell using PE CPE at room temperature.

The inset was Nyquist plots before and after DC polarization.

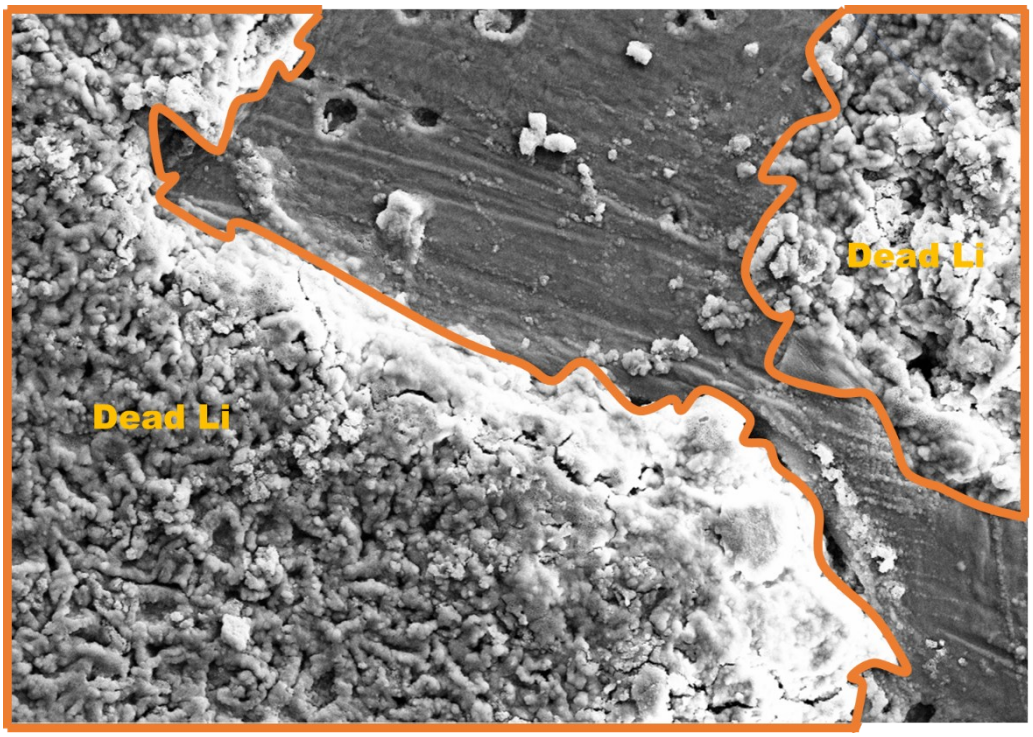

Fig. S13 SEM image of the lithium metal from the Li symmetrical cells using PE-PEG CPE after 700 h cycling at 0.1 mA cm^{-2} and 0.1 mA h cm^{-2}.

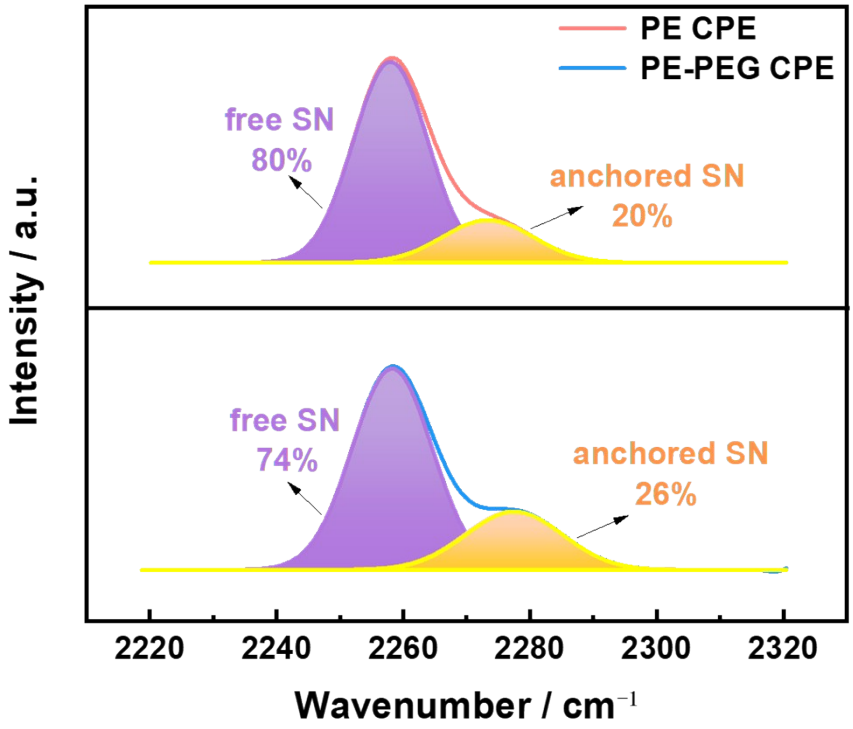

Fig. S14 FTIR spectra of PE CPE and PE-PEG CPE at 2220−2320 cm^{-1}.

We evaluate the rate performance of the Li||PE CPE||Li and Li||PE-PEG CPE||Li cell. The Li||PE CPE||Li cell occurs short circuit at 0.1 mA cm^{-2} and 0.1 mA h cm^{-2} (about 15 h; this result is consistent with the cycling performance at 0.1 mA cm^{-2} and 0.1 mA h cm^{-2}). By contrast, when the current density returns to 0.1 mA cm^{-2}, the Li||PE-PEG CPE||Li cell can still work. The Li||PE-PEG CPE||Li cell shows better rate performance.

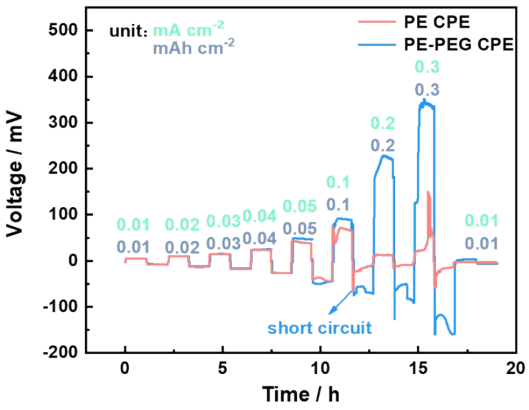

Fig. S15 Rate performance of symmetric cells with PE CPE and PE-PEG CPE.

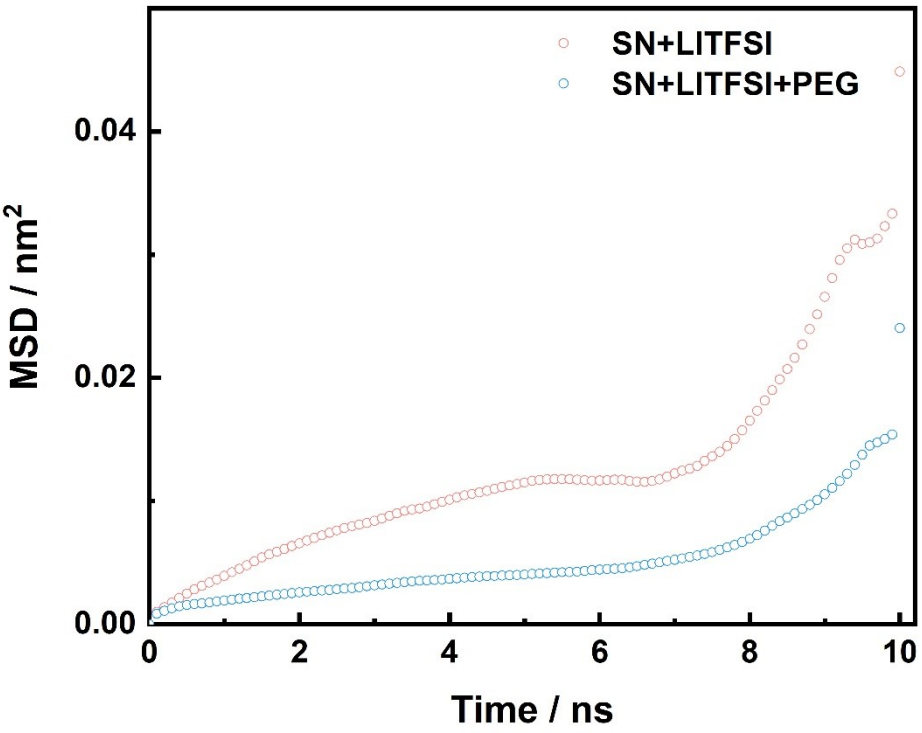

Fig. S16 Mean square displacements (MSDs) of $TFSI^-$ in the two simulated systems.

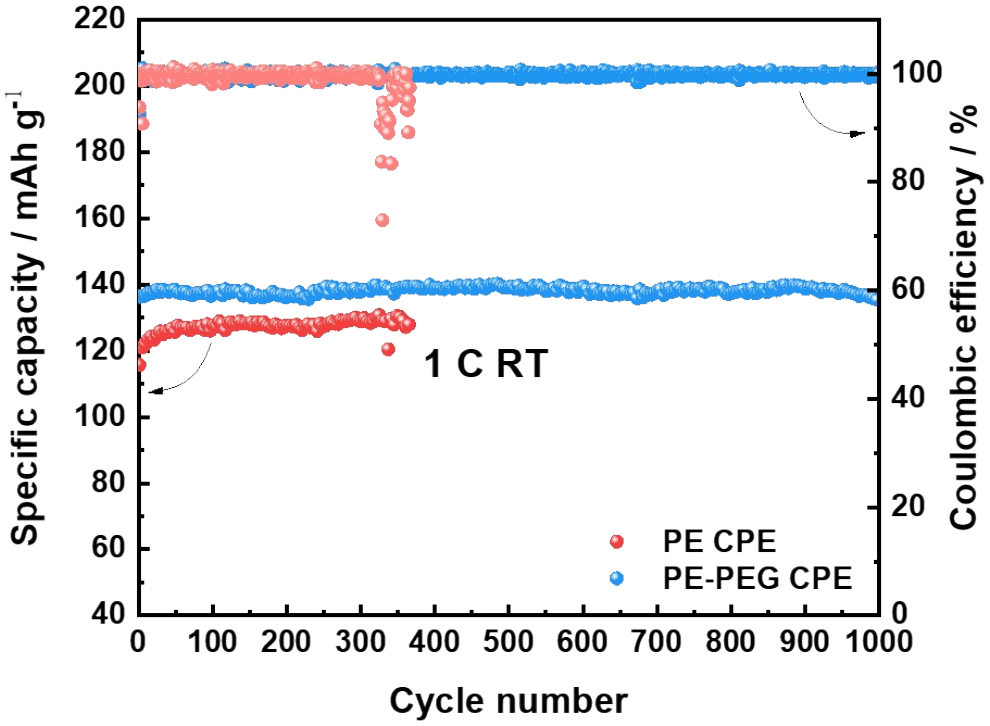

Fig. S17 Cycling performance of solid-state Li||$LiFePO_4$ batteries using PE CPE and PE-PEG CPE at 1 C.

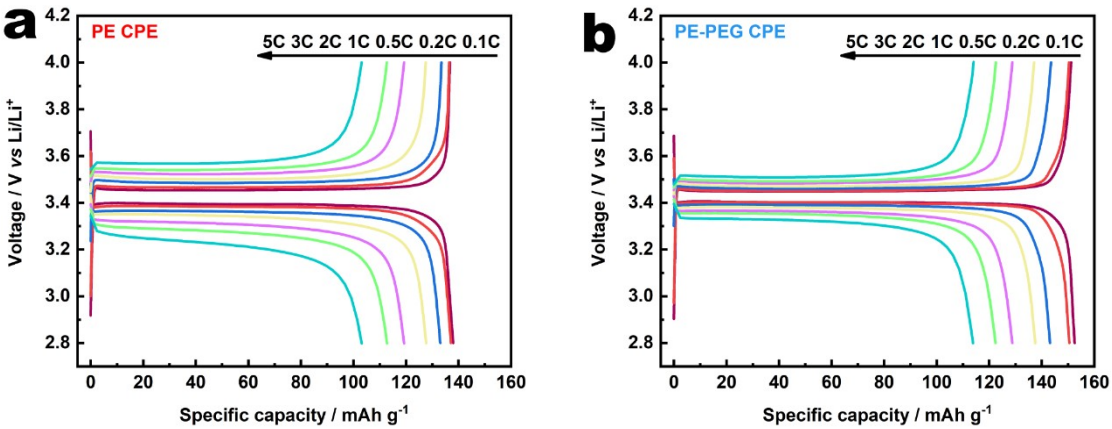

Fig. S18 Charge-discharge curves of solid-state Li||$LiFePO_4$ batteries using a) PE CPE and b) PE-PEG CPE at different rates.

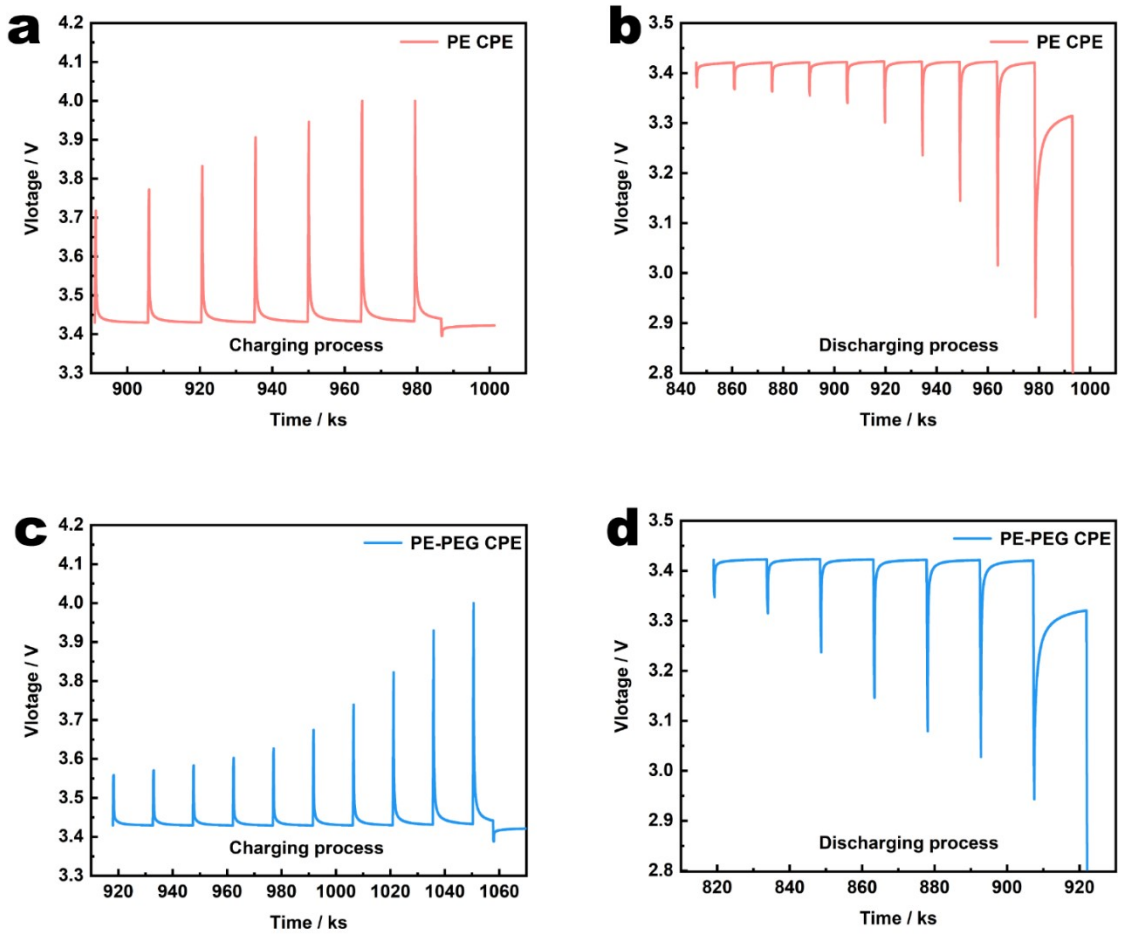

Fig. S19 Galvanostatic intermittent titration technique (GITT) curves of solid-state Li||$LiFePO_4$ batteries with a, b) PE CPE and c, d) PE-PEG CPE during charging and discharging processes at room temperature.

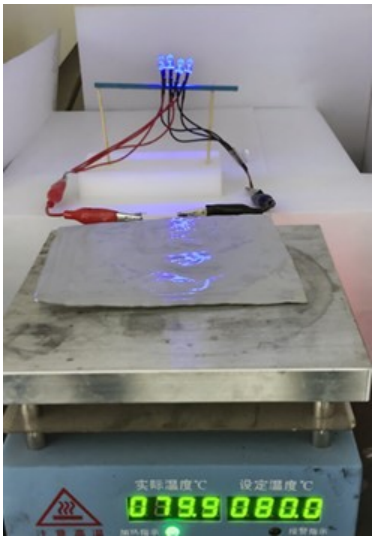

Fig. S20 The reliability and safety of the pouch cell under heating condition.

Table S1 Testing conditions and cycling stability of different SN-based electrolytes by in-situ polymerization reported in literatures.

Monomer	Separator	Cathode/ anode	Temperature	Rate / Cycle life	Reference
ETPTA	PET nonwoven skeleton	$LiFePO_4$/ $Li_4Ti_5O_{12}$	Not mentioned	1C/ 800 cycles	[1]
PVA-CN	PAN based membrane	$LiFePO_4$/ Li	Not mentioned	0.1C/ 100cycles	[2]
CUMA	cellulose membrane	$LiCoO_2$/ Li	30℃	0.5C/ 300cycles	[3]
ETPTA/ mPEGA		$LiFePO_4$/ $Li_4Ti_5O_{12}$	30℃	0.5C/ 1500cycles	[4]
ETPTA	PVDF-HFP membrane	$LiFePO_4$/ Li	25℃	1C/ 800cycles	[5]
ETPTA	PP separator (Celgard 3501)	$LiCoO_2$/ Li	RT	0.5C/ 300cycles	[6]
DOL	PVDF-HFP membrane	$LiFePO_4$/ Li	25℃	2C/ 1000cycles	[7]
BA/ PEGDA	PE or glass fibre separator	$LiFePO_4$/ Li	20℃	1C/ 1000cycles	[8]
ETPTA	PE-PEG	$LiFePO_4$/ Li	RT	3C/ 1000cycles	Our work

Table S2 EIS Simulation results of Figure 4g and Figure 4h.

Battery	After 50 cycles			After 400 cycles		
	$R_b(\Omega)$	$R_f(\Omega)$	$R_{ct}(\Omega)$	$R_b(\Omega)$	$R_f(\Omega)$	$R_{ct}(\Omega)$
LFP|| PE CPE ||Li	**15.32**	**15.32**	**6.99**	**17.6**	**26**	**7.95**
LFP|| PE-PEG CPE||Li	**14.76**	**15.43**	**5.97**	**16.88**	**16.94**	**6.43**

References

1 K. H. Choi, S. J. Cho, S. H. Kim, Y. H. Kwon, J. Y. Kim, S. Y.Lee, *Adv. Funct. Mater.*, 2014,**24** ,44–52.

2 D. Zhou, Y. B. He, R. L. Liu, M. Liu, H. D. Du, B. H. Li, Q. Cai, Q. H. Yang, F. Y. Kang, *Adv. Energy Mater.*, 2015, **5**, 1500353.

3 C. Wang, H. R. Zhang, S. M. Dong, Z. L. Hu, R. X. Hu, Z. Y. Guo, T. Wang, G. L. Cui, L. Q. Chen, *Chem. Mater.*, 2020, **32**, 9167–9175.

4 Z. Yuan, Y. W. Luo, X. Gao, R. Wang, *Chemelectrochem*, 2020, **7**, 2599.

5 W. P. Zha, J. Y. Li, W. W. Li, C. Z. Sun, Z. Y. Wen, *Chem. Eng. J.*, 2021, **406**, 126754.

6 A. X. Wang, S. X. Geng, Z. F. Zhao, Z. L. Hu, J. Y. Luo, *Adv. Funct. Mater.*, 2022, **32**, 2201861.

7 Y. Liu, Y. L.Xu, *Chem. Eng. J.*, 2022, **43**, 134471.

8 M. J. Lee, J. H. Han, K. B. Lee, Y. J. Lee, B. G. Kim, K. N. Jung, B. J. Kim, S. W. Lee, *Nature*, 2022, **601**, 217–222.